Analytical Methods

Accepted Manuscript

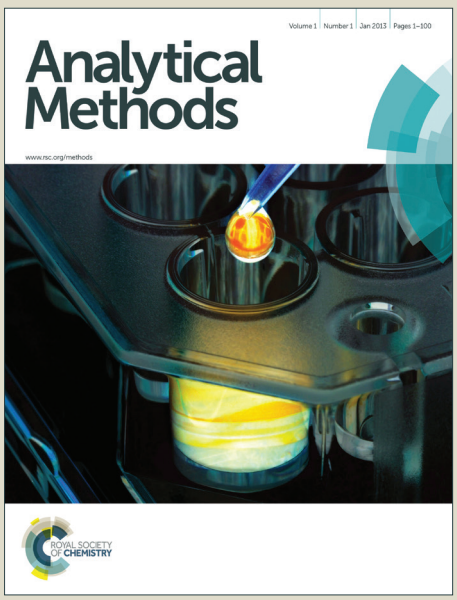

ROYAL SOCIETY OF CHEMISTRY

www.rsc.org/methods

A highly sensitive electrochemical DNA biosensor for rapid detection of CYFRA21-1, a marker of non-small cell lung cancer

Mei Chen[a], Changjun Hou[a,d*],Danqun Huo[a], Mei Yang[a], Huanbao Fa[b]

[a] Key Laboratory of Biorheology Science and Technology, Ministry of Education, College of Bioengineering, Chongqing University, Chongqing 400044, PR China

[b] National Key Laboratory of Fundamental Science of Micro/Nano-Device and System Technology, Chongqing University, Chongqing, 400044, China

[d] College of Chemistry and Chemical Engineering, Chongqing University, Chongqing 400044, China

Abstract: Many studies have confirmed that CYFRA21-1 is both a sensitive and specific marker for non-small cell lung cancer (NSCLC), in particular, squamous cell carcinoma. Therefore, methods to detect CYFRA21-1 are sought to enable early diagnosis. In this manuscript, we report a simple, effective, and convenient method to detect CYFRA21-1 using a novel electrochemical DNA biosensor based on a nanocomposite consisting of carboxyl-functionalized graphene oxide (GO-COOH) and copper oxide nanowires (CuO NWs). The nanocomposite is highly conductive, and was characterized by scanning electron microscopy, transmission electron microscopy, and cyclic voltammetry. Differential pulse voltammetry was also applied to monitor DNA hybridization, using methylene blue as an electrochemical indicator. Under optimal conditions, the biosensor is highly sensitive, with a low detection limit of 1.18×10^{-13} M (at S/N 3). Indeed, CYFRA21-1 could be quantified with good linearity (R^2 = 0.9750) from 1.0×10^{-12} to 1.0×10^{-6} M. The sensor has good stability and selectivity, and discriminates between ssDNA sequences with one- or three-base mismatch. PCR-amplified CYFRA21-1 from a clinical sample was successfully detected, indicating potential application of the biosensor in clinical research and practice.

Keywords: electrochemical DNA biosensor, CYFRA21-1, Carboxyl functionalized graphene oxide, CuO nanowires

1. Introduction

Lung cancer is one of the most serious threats to human health, with the related morbidity and mortality rising worldwide. It is now the leading cause of cancer-related death in the world. The etiology of lung cancer includes several genetic and environmental factors[1].

Tumor biomarkers have been studied extensively as potentially more meaningful measures of chemotherapy response and prognosis. At present, cytokeratin 21-1 (CYFRA21-1) is considered the most important biomarker to detect non-small cell lung cancer (NSCLC), especially squamous cell carcinoma[2]. Indeed, many studies have confirmed the sensitivity and specificity of CYFRA21-1 as a tumor marker. High levels of CYFRA21-1 in the serum are associated with disease progression and relapse in patients with advanced NSCLC [3]. In turn, levels of CYFRA21-1 in the serum have been shown to correlate with steady-state levels of CYFRA21-1 mRNA[4, 5]. Thus, the CYFRA21-1 gene is the most robust DNA-based biomarker for NSCLC.

To date, a variety of techniques have been developed to detect and diagnose DNA sequences associated with cancer, including northern blot, western blot, immunocytochemistry, flow cytometry, and reverse transcriptase-polymerase chain reaction (RT-PCR)[6-8]. However, these techniques suffer from limitations such as lengthy turnaround time, poor precision, technical difficulty, and high cost. Thus, a sensitive, simple, specific, and inexpensive clinical assay for CYFRA21-1 is urgently needed.

DNA biosensors are analytical devices designed to detect a specific target sequence by hybridization with complementary probes immobilized on a solid substrate. Of these biosensors, electrochemical DNA biosensors have attracted considerable attention, because they are selective, easy to use, and cheap to fabricate. In addition, they require inexpensive instrumentation to execute and have rapid turnaround [9-11]. In recent years, a series of nanoparticles have also been exploited to improve sensitivity by increasing surface area, biocompatibility, and conductivity[12, 13]. Indeed, electrode design and probe immobilization are crucial factors that directly affect stability, reproducibility, and sensitivity.

Electrodes for biosensors are frequently functionalized with poly-L-lysine (PLLy) [14], which can be conjugated to the surface by electropolymerization. In this process, L-lysine residues are oxidized to amino free radicals by using high positive potential to catalyze the formation of a carbon-nitrogen bond with a glassy carbon electrode (GCE) surface[15,16].

Graphene (GR) or graphene oxide (GO) has shown promise in various sensor technologies because of high specific surface area, unique structure, and enhanced heat conductance[17-19]. Indeed, many studies have shown that graphene-based electrochemical sensors perform better than traditional electrodes[20]. In particular, GO or GR surfaces functionalized with carboxyl have drawn intense attention in recent years[21]. For instance, covalent attachment of carboxyl functional groups results in remarkable structural effects in GO. In addition, these functional groups can be derivatized and covalently bonded by amidation or esterification with organic molecules, biological macromolecules, and other functional materials[21,22]. Finally, GO-COOH can accommodate various modifications and facilitate electron transfer, and has unique properties, such as one-atom thickness and high specific surface area.

In recent years, sensors have been designed using various composites of graphene and metal oxides as base, including Fe_3O_4-graphene[23], Co_3O_4-graphene[24], MnO_2-graphene[25], and SnO_2-graphene[26]. In particular, copper oxide nanowires (CuO NWs) have been widely used in electrochemical biosensors due to enhanced catalytic, electrical, and magnetic properties, and ability to facilitate electron transfer[27,28]. Recently, various CuO/GO composites, which combine the advantages of GO and CuO to improve electrochemical performance, have been investigated as platforms for catalysis, microelectronics, chemical and biological sensing [29,30]. However, DNA or nucleic acid hybridization on CuO/GO-COOH nanocomposites has not been reported.

In this study, we combine the advantages of L-lysine, GO-COOH, and CuO NWs to develop a facile and sensitive electrochemical DNA biosensor to detect CYFRA21-1. In addition to advantages derived from individual components, the nanocomposite has the following features: (1) the GCE is functionalized with PLLy, is abundantly coated with NH_2, and electrostatically adsorbs negatively charged nanosheets comprised of GO-COOH and CuO NWs; (2) the GO-COOH component has excellent electrochemical redox active properties, and also act as a “bridge” to connect composite materials to the PLLy/GCE surface, and to immobilize DNA probes through formation of amide bonds with NH_2-ssDNA; (3) the nanocomposite is easily and rapidly fabricated; and (4) electron transfer is synergistically enhanced in nanosheets, in which CuO NWs are woven into a mesh with GO-COOH. The new electrochemical DNA biosensor is easy to use, and successfully detects CYFRA21-1 with high selectivity and broad linear range. The fabrication and use of the biosensor are illustrated in Scheme 1.

2. Experimental

2.1. Apparatus and reagents

Electrochemical measurements were performed on a CHI660D electrochemical workstation (Shanghai Chenhua Instruments Co. Ltd., China) with a conventional three-electrode system composed of platinum as auxiliary, silver/silver chloride (Ag/AgCl) as reference, and a GCE or a modified GCE as working electrode. Fourier-transform infrared (FT-IR) spectra were collected on a Tensor 27 FT-IR spectrophotometer (Bruker, Germany). Morphology was examined on a JEM 2100 transmission electron microscope (TEM) and a Hitachi S-4800 scanning electron microscope (SEM).

Probe and target oligonucleotides, with the following sequences, were synthesized and purified by Sangon Biological Engineering Tech. Co. Ltd. (Shanghai, China):

probe: NH_2-GAAGGGAGGAATGGTGTCAGGGGCG

perfectly complementary target: CGCCCCTGACACCATTCCTCCCTTC

target with one-base mismatch: CGCCCCTGACTCCATTCCTCCCTTC

target with three-base mismatch: CGCGCCTGACTCCATTCCTCCCATC

non-complementary target: TTGTCCAGGTAGGAGGCCAGGCGGT

The DNA template for polymerase chain reaction was extracted from lung cancer tissues. PCR was carried out in an Eppendorf Mastercycler Gradient PCR system, and gel images were recorded on a Bio-Rad imaging system (Bio-Rad Laboratories, USA). CYFRA21-1 was amplified with the following primers:

forward: GAAGGGAGGAATGGTGTCAGGGGCG

reverse: CGCCCCTGACACCATTCCTCCCTTC

N-(3-dimethyl-amino-propyl)-N'-ethylcarbodiimide hydrochloride (EDC) and sodium dodecyl sulfate (SDS) were purchased from Sigma (USA). N-hydroxy-succinimide (NHS) was obtained from Shanghai Medpep Co. Ltd. (China). L-lysine and methylene blue (MB) were procured from Shanghai Zheng xiang (China) and Shanghai Chemicals Plant (China), respectively. All reagents were analytical grade.

The following buffers were prepared with doubly distilled water: 0.2 M PBS (pH 8.0), 50.0

mM PBS (pH 7.0), and 50.0 mM Tris-HCl (pH 7.0).

2.2. Synthesis of carboxyl functionalized graphene oxide

GO was prepared from graphite flakes following the method described by Hummers[31-33], with some modification. The GO was then carboxylated according to a published method[34]. In brief, 1.2 g NaOH was added to 5.0 mL of 2.0 mg mL^{-1} GO solution, and the suspension was sonicated for 2 h. Subsequently, 10 mg chloroacetic acid was added, and the mixture was sonicated for 2 h to conjugate acetic acid moieties to hydroxyl groups, yielding carboxyl functionalized graphene oxide (GO-COOH)[35]. Finally, the GO-COOH suspension was alkalinized to neutral pH, and purified by repeated rinsing and filtration.

2.3. Preparation of CuO/GO-COOH nanocomposites

CuO NWs were prepared by thermal oxidation of Cu nanowires (Cu NWs), which were fabricated following a method reported elsewhere[36,37]. Briefly, 20 mL 15 M NaOH was preheated to 60°C, at which 1 mL 0.1 M $Cu(NO_3)_2$, 0.16 mL EDA, and 25 µL 35 wt% N_2H_4 were sequentially added. The reaction was incubated at 60°C for another 2 h. The resulting reddish Cu NWs were directly calcined at 400°C for 5 h to obtain CuO NWs. The product, black CuO NWs, was suspended in ethanol to a concentration of 2 mg/mL. The nanocomposite was prepared by simply mixing GO-COOH and CuO NWs at a volumetric proportion of 1:1, and then sonicating to homogeneity.

2.4. Fabrication of modified electrodes

A glassy carbon electrode was first polished with alumina powder, rinsed with water, and sonicated in ethanol and then in distilled water. The polished GCE was then air-dried at room temperature, and coated with L-lysine according to published methods[14,38]. Subsequently, the GCE was placed in 0.2 M PBS pH 8.0 supplemented with 0.01 M L-lysine, and subjected to 10 cycles of cyclic voltammetric scans from -1.0 to 2.2 V at scan rate 100 mV s^{-1}. The electrode was then thoroughly rinsed with doubly distilled water and then air dried at room temperature to obtain PLLy-modified GCE. Finally, 5.0 µL suspension of GO-COOH and CuO nanowires was spotted onto the GCE surface, which was then dried in air.

2.5. Immobilization of probe ssDNA

The modified electrode was immersed for 40 min in a solution of 5.0 mM EDC and 8.0 mM NHS to activate the carboxyl group. Subsequently, the electrode was incubated for 2 h at room

temperature with 5 μL probe ssDNA (1×10^{-6} M). The probe ssDNA contains an amine group at the 5' end, and is covalently linked to the electrode via an amide bond. Finally, the electrode was washed with 0.1% SDS in PBS pH 7.0 to eliminate unconjugated ssDNA.

2.6. Hybridization with target ssDNA

Electrodes were hybridized for 60 min at room temperature with 5.0 μL target ssDNA prepared at different concentrations in 50.0 mM PBS. To remove unhybridized targets, the electrode was then rinsed with 0.5% SDS and then with doubly distilled water.

2.7. Characterization and electrochemical detection

After hybridization, the electrode was immersed in 5.0 mL methylene blue for 15 min. Methylene blue intercalates into dsDNA, and thus accumulates on the electrode surface. The electrode was then washed several times with 0.5% SDS and water to remove nonspecifically adsorbed methylene blue. The electrochemical response due to methylene blue was measured by differential pulse voltammetry in 50.0 mM Tris-HCl buffer pH 7.0 with pulse amplitude 0.008 V, pulse width 0.05 s, and pulse period 0.2 s.

2.8. Preparation of DNA samples and PCR

Genomic DNA was extracted from lung cancer tissue by Wizard Genomic DNA Purification Kit (Promega-USA) following the manufacturer's instructions, and used directly as PCR template.

CYFRA21-1 gene fragments were amplified in a final reaction volume of 25 μL. Reactions contained 200.0 nM each of forward and reverse primer, 1× reaction buffer B (Promega, Wisconsin USA), 2.0 mM $MgCl_2$, 200.0 nM each of dNTP, 1.5 units Taq DNA polymerase (Promega, Wisconsin USA), and 1.0 μL template DNA. PCR parameters were as follows: (i) initial denaturation at 94°C for 3 min, (ii) 34 cycles of denaturation at 95°C for 1 min, annealing at 55°C for 1 min, and extension at 72°C for 1 min, and (iii) final extension at 72°C for 10 min. PCR products were visualized under ultraviolet light after running 6 μL of the reaction mixture on 2% agarose gel containing 1 mg mL^{-1} ethidium bromide.

3. Results and discussion

3.1. Characterization of the hybrid composite of GO-COOH and CuO NWs

Fig. 1A and B show typical transmission electron microscopy (TEM) images of GO-COOH and its composite with CuO NWs, as fabricated. It is clear that GO-COOH has the typical

appearance of crumpled planar sheets, indicating that the material was readily exfoliated into individual sheets by ultrasonic treatment in water (Fig. 1A). On the other hand, CuO NWs formed a dense network adsorbed on GO-COOH sheets, indicating a homogeneous composite with complete and uniform mixing of components (Fig. 1B).

The hybrid composite was also characterized by scanning electron microscopy (SEM). As can be seen in Fig. 1C, CuO NWs are well dispersed on the GO-COOH surface and form an interconnected network that provides a feasible pathway for electron transfer.

To further characterize the materials and probe the nature of functional groups on the surface, FTIR spectra were collected (Fig. 1D). In GO-COOH, a strong broad peak at 3444.5 cm^{-1} corresponds to stretching vibration of O-H. Peaks at 1722 cm^{-1} and 1624.0 cm^{-1} are characteristic of C=O and C=C stretching vibration, respectively. In CuO NWs, adsorption at 513.3 cm^{-1} and 592.7 cm^{-1} denotes stretching vibration of the Cu-O bond[39,40]. Additional adsorption peaks may be due to O-H bending vibration in some constitutional water incorporated into the nanowire. In the composite material, characteristic peaks of both components are observed. However, the intensities of these peaks are diminished, reflecting lower concentration in the composite than in pure samples. Thus, FTIR spectra confirm attachment of CuO NWs to the surface of GO-COOH sheets.

3.2. Electrochemical characterization

Cyclic voltammetry is an effective and convenient method to characterize modified electrode surfaces. Using 1.0 mM $[Fe(CN)_6]^{3-/4-}$ in 0.1 M KCl and a scan rate of 100 mV s^{-1}, we characterized bare GCE, GCE functionalized with PLLy, functionalized GCE coated with GO-COOH, and functionalized GCE coated with CuO/GO-COOH (Fig. 2). In comparison to bare GCE (curve a), a small decrease in peak current is observed when the surface is electropolymerized with PLLy (curve b). When GO-COOH was immobilized on the surface of GCE, the peak current clearly increased (curve c), indicating that the nanosheet has large surface area and excellent conductivity. Finally, incorporation of CuO NWs into GO-COOH resulted in a prominent peak (curve d), indicating significantly accelerated electron transfer of $[Fe(CN)_6]^{3-/4-}$. These results indicate that a nanocomposite of GO-COOH and CuO is an efficient conducting material, and would improve the sensitivity of the biosensor. The enhanced conductivity can be directly attributed to good electronic performance of CuO NWs and the formation of entangled

CuO/GO-COOH porous and mesh structures. The reversibility and peak current of $[Fe(CN)_6]^{3-/4-}$ decreased after probe DNA was immobilized on CuO/GO-COOH/PLLy/GCE (curve e). This was due to electrostatic repulsion between negatively charged NH_2-ssDNA and $[Fe(CN)_6]^{3-/4-}$. These results indicate that a working DNA sensor has been successfully fabricated.

3.3. Optimization of experimental conditions

The biosensor is operated on the basis of a current of methylene blue (MB), which binds double-stranded DNA and functions as an indicator of hybridization. To optimize detection of target DNA, operational conditions were investigated, including the ratio of CuO NWs to GO-COOH, hybridization time and temperature, as well as concentration of and incubation time with MB.

As shown in Fig. 3A, a ratio of 1:1 (v/v) CuO NWs:GO-COOH gives the highest peak current. Thus, this ratio was selected for subsequent experiments. The effect of hybridization temperature was tested in the range 25-60 °C. the largest peak current occurred at 35 °C (Fig. 3B). Therefore, hybridization temperature was fixed at 35 °C. At this temperature, the peak current obviously increased with hybridization time from 30 to 60 min, and stabilized thereafter (Fig. 3C). This result indicates that hybridization is essentially complete after 60 min. Thus, 60 min was set as optimum hybridization time.

To maximize efficiency and sensitivity, we optimized the concentration of and incubation time with MB. We found the current to increase with MB concentration between 5.0×10^{-6} M and 2.5×10^{-5} M, and plateaued thereafter (Fig. 3D). Therefore, the sensor was subsequently operated at 2.5×10^{-5} M MB. The peak current also increased significantly with incubation time from 0 to 15 min (Fig. 3E). Thus, incubation time with MB was set at 15 min, after which no additional increase in current is observed. This result indicates that most MB molecules intercalate into double-stranded DNA within 15 min.

3.4. Sensitivity at different concentrations of target ssDNA

Sensitivity was investigated under optimal experimental conditions, by hybridization with different concentrations of synthetic target ssDNA. Increasing concentration of target ssDNA will hybridize with increasing amounts of probe ssDNA to form increasing amounts of dsDNA. In turn, the increased density of dsDNA will result in accumulation of more MB and generate a stronger electrochemical response. As shown in Fig. 4, the reduction peak current of MB increased

gradually with increasing concentrations of target ssDNA. Indeed, the peak current was linear with the logarithm of target ssDNA concentration from 1.0×10^{-12} M to 1.0×10^{-6} M. The corresponding regression equation was ΔI (μA) = 1.946 log C (M) + 23.95 with correlation coefficient 0.9750. The detection limit, estimated as three times the standard deviation of the blank, was calculated to be 1.18×10^{-13} M. The linear range and detection limit of this biosensor were compared with published values from similar experiments (Table 1), and show that the DNA sensor has good analytical performance.

3.5. Selectivity

Selectivity is a critical parameter in a DNA biosensor. The selectivity of our biosensor was determined using four targets, including a non-complementary strand, a strand with three bases mismatched, a sequence with one base mismatched, and a perfectly complementary target. Performance was evaluated at 1.0×10^{-7} M. As shown in Fig. 5, a low peak current was observed when the sensor was hybridized with a noncomplementary target (curve b), indicating minimal or zero hybridization. However, the peak current increased significantly after hybridization with sequences containing 3- (curve c) and 1-base (curve d) mismatch. The increase in current clearly suggests hybridization between the probe and mismatched targets. However, the peak current was higher when the mismatch was only one base instead of three, suggesting that the sensor distinguishes between these sequences. Finally, the current was highest when a perfectly complementary target was used (curve e). These results demonstrate that the biosensor has high selectivity.

3.6. Reproducibility and stability

To evaluate the reproducibility of the DNA sensor, a series of five electrodes were fabricated, and tested against 0.1 nM target sequence. Measurements on five electrodes were highly reproducible, with relative standard deviation (RSD) 4.6%. Stability was also investigated, and results indicate that the ssDNA sequence is stably immobilized on the electrode surface due to covalent linkage. After 14 days of storage at 4°C, 97.2% of the initial sensitivity remained, indicating this modified electrode was a stable platform as electrochemical DNA biosensor.

3.7. Evaluation with a clinical sample

Performance was examined using CYFRA21-1 from a clinical sample of lung cancer tissue. After pretreatment of genomic extracts, the gene was amplified by PCR, and products were

electrophoresed on agarose gel (Fig. 6A). The PCR product migrated at the expected size of 1490 bp.

To obtain ssDNA, amplified CYFRA21-1 was diluted 1:10 with 50.0 mM PBS, and denatured for 5 min at 95 °C in a water bath, and then cooled in an ice bath for 1 min. The sensor was hybridized and operated as described using 5.0 µL ssDNA (Fig. 6B). The peak current increased significantly upon hybridization with PCR-amplified CYFRA21-1 (curve c), indicating presence of target DNA. However, hybridization with products from a PCR reaction without template DNA (curve b) increased the current only slightly above blank (curve a).

These results indicate that PCR produced many copies of the target sequence. As a result, hybridization with the sensor formed dsDNA molecules on the electrode surface, and generated the strongest signal. The small increase between curve b and curve a may have been caused by non-specific adsorption of PCR primers. The significant difference between blank and the sensor hybridized with amplified CYFRA21-1 confirms that the gene could be effectively detected in clinical samples.

4. Conclusions

This paper describes the design and fabrication of a novel electrochemical biosensor for rapid detection of CYFRA21-1, the most important DNA biomarker for NSCLC. The biosensor is fabricated by covalent immobilization of probe ssDNA, through amide bonds, on a GCE functionalized with PLLy and coated with a nanocomposite of GO-COOH and CuO NWs. Due to the large specific area of GO-COOH and good conductivity of CuO, the biosensor is a promising diagnostic platform with high sensitivity and low detection limit. The performance of the biosensor was evaluated using synthetic oligonucleotides and PCR products of CYFRA21-1 from a patient with a confirmed diagnosis.

More generally, this work establishes a framework for developing DNA biosensors with good analytical properties. However, to fully assess the potential and value of this class of biosensors, future research should focus on other target sequences and sample types. Indeed, we believe that more research is needed to generate a reliable, robust, and sensible microchip technology to analyze nucleic acids in clinical samples rapidly. Future efforts in our laboratory will be directed towards this goal.

Acknowledgment

The authors would like to acknowledge the financial support from the National Natural Science Foundation of China (NSFC) (81171414, 81271930), Chongqing Graduate Student Research Innovation Project (CYB14028), Key Technologies R&D Program of China (2012BAI19B03) and sharing fund of Chongqing university's large equipments.

References:

1. J. E. Tota, A. V. Ramanakumar and E. L. Franco, *Lung*, 2014, **192**, 55-63.
2. S. Holdenrieder, J. von Pawel, E. Dankelmann, T. Duell, B. Faderl, A. Markus, M. Siakavara, H. Wagner, K. Feldmann, H. Hoffmann, H. Raith, D. Nagel and P. Stieber, *Lung cancer*, 2009, **63**, 128-135.
3. F. Barlési, C. Gimenez, J.-P. Torre, C. Doddoli, J. Mancini, L. Greillier, F. Roux and J.-P. Kleisbauer, *Resp Med* , 2004, **98**, 357-362.
4. J. L. Pujol, J. M. Boher, J. Grenier and X. Quantin, *Lung cancer*, 2001, **31**, 221-231.
5. N. Reinmuth, B. Brandt, M. Semik, W. P. Kunze, R. Achatzy, H. H. Scheld, P. Broermann, W. E. Berdel, H. N. Macha and M. Thomas, *Lung cancer*, 2002, **36**, 265-270.
6. P. Hokland and N. Pallisgaard, *Semin Hematol*, 2000, **37**, 358-367.
7. L. H. Olesen, J. M. Norgaard, N. Pallisgaard, A. Bukh and P. Hokland, *Eur J Haematol*, 2003, **70**, 296-303.
8. H. Tamaki, M. Mishima, M. Kawakami, A. Tsuboi, E. H. Kim, N. Hosen, K. Ikegame, M. Murakami, T. Fujioka, T. Masuda, Y. Taniguchi, S. Nishida, K. Osumi, T. Soma, Y. Oji, Y. Oka, I. Kawase, H. Sugiyama and H. Ogawa, *Int J Hematol*, 2003, **78**, 349-356.
9. K. J. Feng, Y. H. Yang, Z. J. Wang, J. H. Jiang, G. L. Shen and R. Q. Yu, *Talanta*, 2006, **70**, 561-565.
10. K.-J. Huang, Y.-J. Liu, H.-B. Wang and Y.-Y. Wang, *Electrochim Acta* , 2014, **118**, 130-137.
11. A. Singh, G. Sinsinbar, M. Choudhary, V. Kumar, R. Pasricha, H. N. Verma, S. P. Singh and K. Arora, *Sens Actuator B Chem* , 2013, **185**, 675-684.
12. M. L. Yola, T. Eren and N. Atar, *Electrochim Acta* , 2014, **125**, 38-47.
13. L. Zhu, L. Luo and Z. Wang, *Biosens Bioelectron*, 2012, **35**, 507-511.
14. J. Wang, S. Zhang and Y. Zhang, *Anal Biochem* , 2010, **396**, 304-309.
15. S. C. C. Monterroso, H. M. Carapuca and A. C. Duarte, *Talanta*, 2006, **68**, 1655-1662.
16. H. Katano, K. Uematsu, C. Maruyama and Y. Hamano, *Anal Sci*, 2014, **30**, 17-24.
17. V. K. Gupta, M. L. Yola, M. S. Qureshi, A. O. Solak, N. Atar and Z. Üstündağ, *Sens Actuator B Chem* , 2013, **188**, 1201-1211.
18. H. Y. He, J. Klinowski, M. Forster and A. Lerf, *Chem Phys Lett*, 1998, **287**, 53-56.
19. Y. J. Song, K. G. Qu, C. Zhao, J. S. Ren and X. G. Qu, *Adv Mater*, 2010, **22**, 2206-2210.
20. M. Muti, S. Sharma, A. Erdem and P. Papakonstantinou, *Electroanal*, 2011, **23**, 272-279.
21. K. J. Huang, D. J. Niu, J. Y. Sun, C. H. Han, Z. W. Wu, Y. L. Li and X. Q. Xiong, *Colloid Surface B* , 2011, **82**, 543-549.
22. K. W. Park and J. H. Jung, *J Power Sources*, 2012, **199**, 379-385.
23. H. He and C. Gao, *ACS Appl Mater Interfaces*, 2010, **2**, 3201-3210.

24. X. W. Wang, S. Q. Liu, H. Y. Wang, F. Y. Tu, D. Fang and Y. H. Li, *J Solid State Electr*, 2012, **16**, 3593-3602.
25. C. X. Guo, M. Wang, T. Chen, X. W. Lou and C. M. Li, *Adv Energy Mater*, 2011, **1**, 736-741.
26. C. Z. Zhu, Y. X. Fang, D. Wen and S. J. Dong, *J Mater Chem*, 2011, **21**, 16911-16917.
27. L. C. Jiang and W. D. Zhang, *Biosens Bioelectron*, 2010, **25**, 1402-1407.
28. T. Li, X. P. Ai and H. X. Yang, *J Phys Chem C*, 2011, **115**, 6167-6174.
29. T. Alizadeh and S. Mirzagholipur, *Sens Actuator B Chem* , 2014, **198**, 438-447.
30. X. L. Wang, E. L. Liu and X. L. Zhang, *Electrochim Acta*, 2014, **130**, 253-260.
31. L. J. Cote, F. Kim and J. X. Huang, *J Am Chem Soc*, 2009, **131**, 1043-1049.
32. N. I. Kovtyukhova, P. J. Ollivier, B. R. Martin, T. E. Mallouk, S. A. Chizhik, E. V. Buzaneva and A. D. Gorchinskiy, *Chem Mater*, 1999, **11**, 771-778.
33. M. X. Wang, Q. Liu, H. F. Sun, E. A. Stach, H. Y. Zhang, L. Stanciu and J. Xie, *Carbon*, 2012, **50**, 3845-3853.
34. X. M. Sun, Z. Liu, K. Welsher, J. T. Robinson, A. Goodwin, S. Zaric and H. J. Dai, *Nano Res*, 2008, **1**, 203-212.
35. M. Hallbeck, O. Hermanson and A. Blomqvist, *Neurosci Lett*, 1996, **209**, 125-128.
36. Y. C. Zhang, L. Su, D. Manuzzi, H. V. E. de los Monteros, W. Z. Jia, D. Q. Huo, C. J. Hou and Y. Lei, *Biosens Bioelectron*, 2012, **31**, 426-432.
37. Y. Chang, M. L. Lye and H. C. Zeng, *Langmuir*, 2005, **21**, 3746-3748.
38. W. Zhao, X. Q. Wu, Z. Q. Lu, W. J. Hou and H. X. Li, *Chinese Chem Lett*, 2010, **21**, 93-96.
39. D. P. Dubal, D. S. Dhawale, R. R. Salunkhe, V. S. Jamdade and C. D. Lokhande, *J Alloy Compd*, 2010, **492**, 26-30.
40. A. Pendashteh, M. F. Mousavi and M. S. Rahmanifar, *Electrochim Acta* , 2013, **88**, 347-357.
41. S. Niu, M. Zhao, R. Ren and S. Zhang, *J Inorg Biochem*, 2009, **103**, 43-49.
42. Y. Bo, H. Yang, Y. Hu, T. Yao and S. Huang, *Electrochim Acta*, 2011, **56**, 2676-2681.
43. K. Jayakumar, R. Rajesh, V. Dharuman, R. Venkatasan, J. H. Hahn and S. K. Pandian, *Biosens Bioelectron*, 2012, **31**, 406-412.
44. D. S. Campos-Ferreira, G. A. Nascimento, E. V. Souza, M. A. Souto-Maior, M. S. Arruda, D. M. Zanforlin, M. H. Ekert, D. Bruneska and J. L. Lima-Filho, *Anal Chim Acta*, 2013, **804**, 258-263.
45. H.-P. Peng, Y. Hu, P. Liu, Y.-N. Deng, P. Wang, W. Chen, A.-L. Liu, Y.-Z. Chen and X.-H. Lin, *Sens Actuator B Chem*, 2015, **207**, 269-276.

Scheme 1. Fabrication and detection process of the DNA biosensor.

Fig. 1. (A) TEM image of GO-COOH. (B) TEM and (C) SEM images of a composite of GO-COOH and CuO. (D) FT-IR spectra of (a) CuO nanowires, (b) GO-COOH, and (c) composite of GO-COOH and CuO.

Fig. 2. Cyclic voltammetry, using 1.0 mM $Fe(CN)_6^{3-/4-}$, of (a) bare GCE, (b) GCE functionalized with PLLy, (c) functionalized GCE coated with GO-COOH, (d) functionalized GCE coated with a composite of GO-COOH and CuO, and (e) GCE/nanocomposite decorated with ssDNA probe.

Fig. 3. Effects of (A) the ratio of CuO to GO-COOH, (B) hybridization temperature, (C) hybridization time, (D) MB concentration, and (E) incubation time.

Fig. 4. DPV curves after hybridization with 0 M, 1.0×10^{-12} M, 1.0×10^{-11} M, 1.0×10^{-10} M, 1.0×10^{-9} M, 1.0×10^{-8} M, 1.0×10^{-7} M and 1.0×10^{-6} M target ssDNA (curves a-h, respectively). Inset, plot of peak current vs. log of the concentration of target ssDNA.

Fig. 5. Selectivity of the biosensor. DPV curves (a) without target ssDNA, and after hybridization with 1.0×10^{-6} M (b) noncomplementary ssDNA, (c) ssDNA with 3-base or (d) 1-base mismatch, and (e) complementary ssDNA.

Fig. 6. (A) PCR-amplified CYFRA21-1. (B) Electrochemical response (a) without target DNA, or in the presence of PCR products amplified (b) without or (c) with template DNA from a clinical sample.

Table 1

Comparison of the linear range and detection limit of electrochemical DNA sensors.

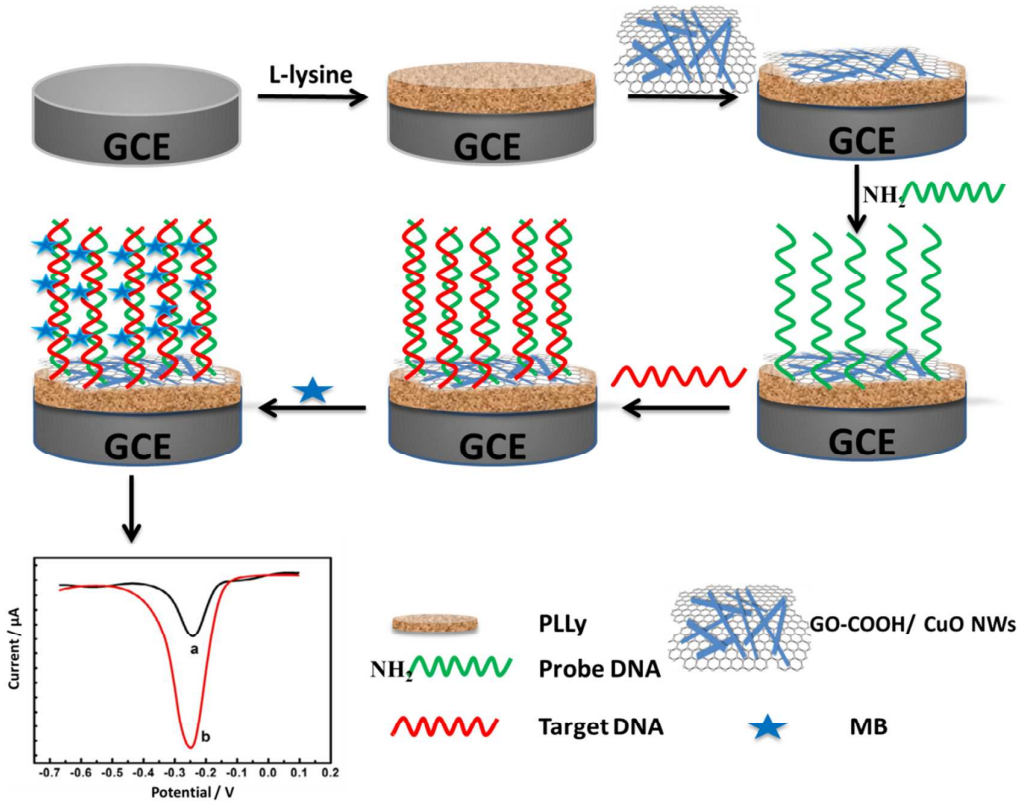

Scheme 1. Fabrication and detection process of the DNA biosensor.

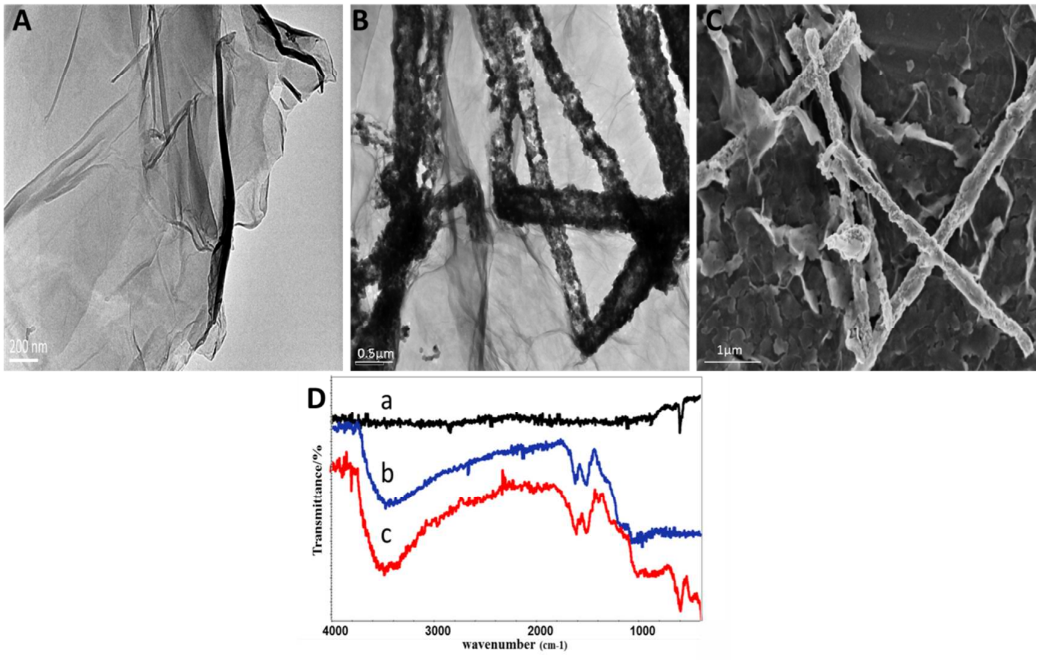

Fig. 1.

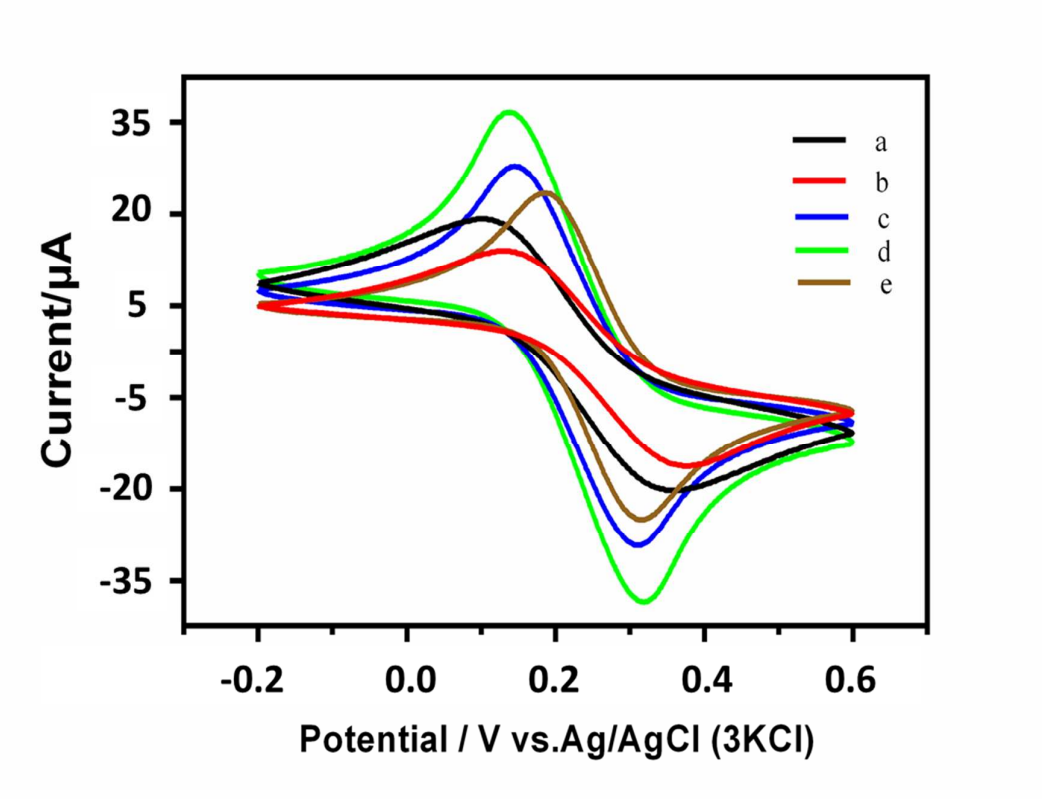

Fig. 2. Cyclic voltammetry, using 1.0 mM $Fe(CN)_6^{3-/4-}$, of (a) bare GCE, (b) GCE functionalized with PLLy, (c) functionalized GCE coated with GO-COOH, (d) functionalized GCE coated with a composite of GO-COOH and CuO, and (e) GCE/nanocomposite decorated with ssDNA probe.

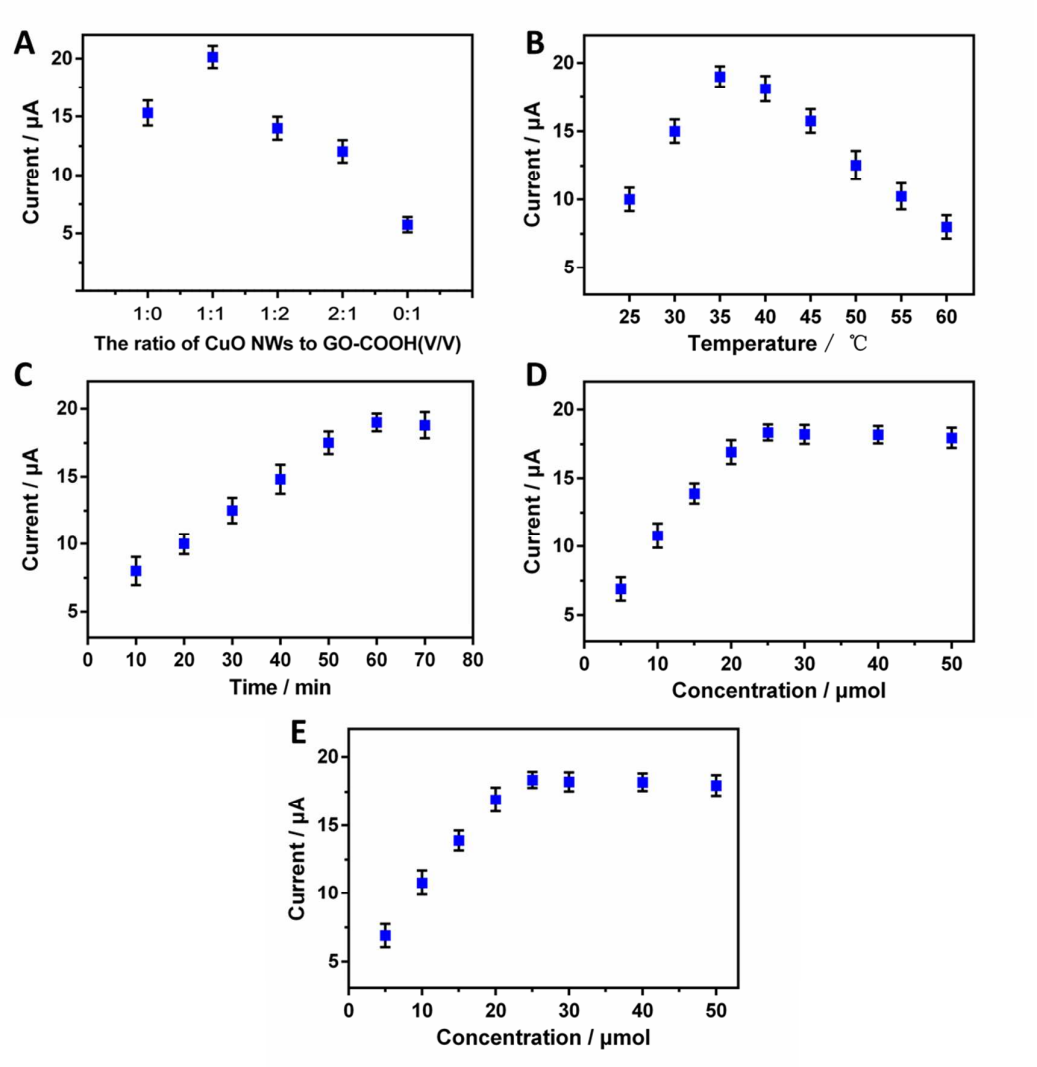

Fig. 3. Effects of (A) the ratio of CuO to GO-COOH, (B) hybridization temperature, (C) hybridization time, (D) MB concentration, and (E) incubation time.

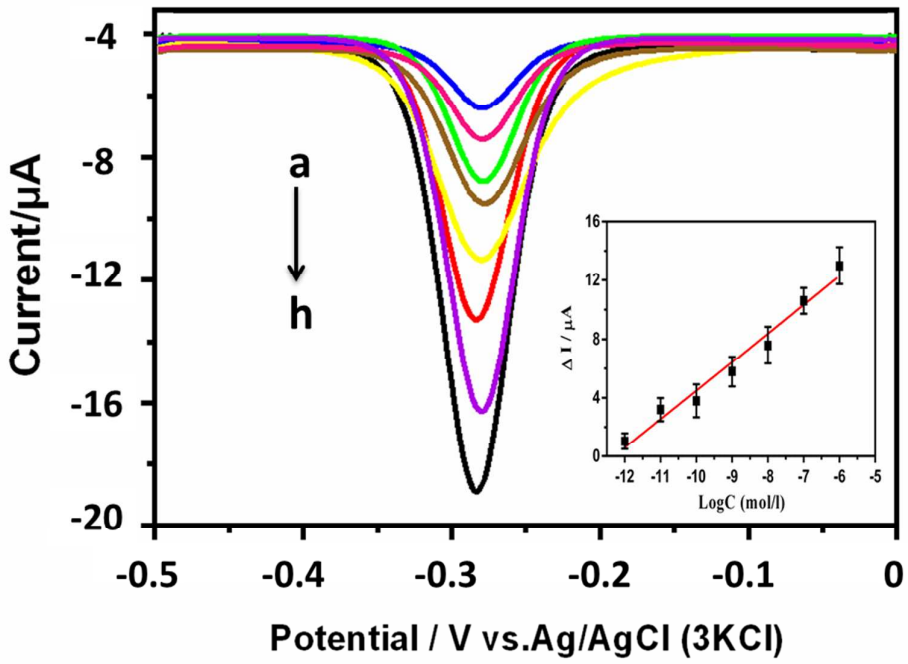

Fig. 4. DPV curves after hybridization with 0 M, 1.0×10^{-12} M, 1.0×10^{-11} M, 1.0×10^{-10} M, 1.0×10^{-9} M, 1.0×10^{-8} M, 1.0×10^{-7} M and 1.0×10^{-6} M target ssDNA (curves a-h, respectively). Inset, plot of peak current vs. log of the concentration of target ssDNA.

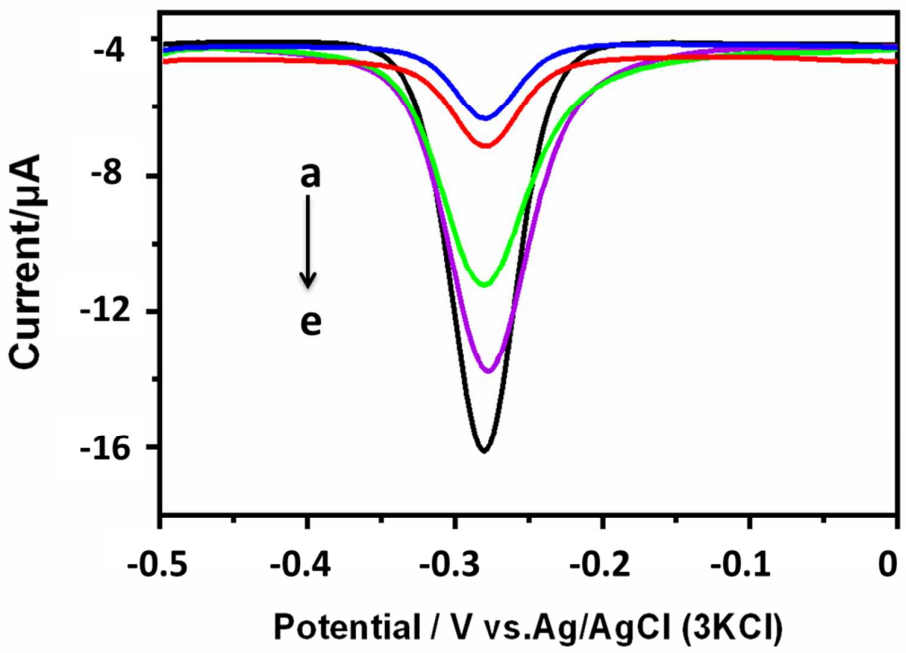

Fig. 5. Selectivity of the biosensor. DPV curves (a) without target ssDNA, and after hybridization with 1.0×10^{-6} M (b) noncomplementary ssDNA, (c) ssDNA with 3-base or (d) 1-base mismatch, and (e) complementary ssDNA.

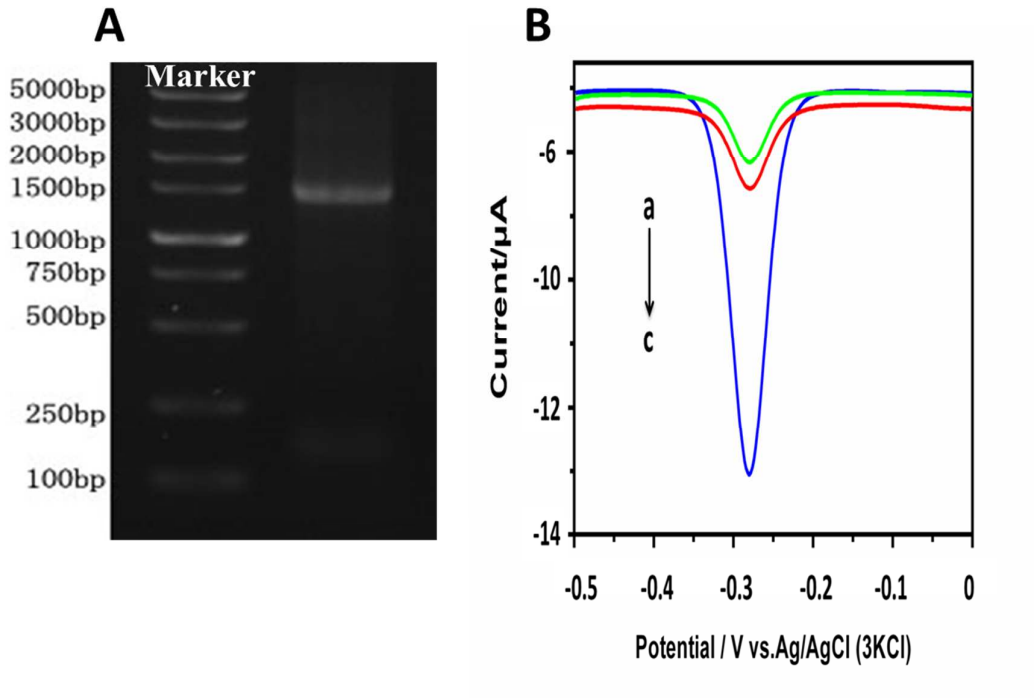

Fig. 6. (A) PCR-amplified CYFRA21-1. (B) Electrochemical response (a) without target DNA, or in the presence of PCR products amplified (b) without or (c) with template DNA from a clinical sample.

Table 1

Comparison of the linear range and detection limit of electrochemical DNA sensors.

Modified electrodes	Detection technique	Linear range (M)	Detection limit (M)	References
MWCNTs-COOH	DPV	1.6×10^{-9}-4.8×10^{-8}	3.8×10^{-11}	41
Graphene/polyaniline nanowires	CV	2.12×10^{-12}-2.12×10^{-6}	3.25×10^{-13}	42
MPA-GG_1PAMAM-Au nano	DPV	1.0×10^{-12}-1.0×10^{-6}	1.75×10^{-10}	43
L-Cysteine	DPV	2.5×10^{-11}-1.87×10^{-10}	1.83×10^{-10}	44
Au NPs/TB-GO	DPV	1.0×10^{-11}-1.0×10^{-9}	2.9×10^{-12}	45
CuO/GO-COOH/PLLy	DPV	1.0×10^{-12}-1.0×10^{-6}	1.18×10^{-13}	This work